JOURNAL OF THE AMERICAN CHEMICAL SOCIETY

Article

pubs.acs.org/JACS

Controlled Synthesis and Magnetic Properties of Bimagnetic Spinel Ferrite $CoFe_2O_4$ and $MnFe_2O_4$ Nanocrystals with Core–Shell Architecture

Qing Song[§] and Z. John Zhang*

School of Chemistry & Biochemistry, Georgia Institute of Technology, Atlanta, Georgia 30332-0400, United States

ABSTRACT: A combination of hard phase $CoFe_2O_4$ and soft phase $MnFe_2O_4$ as the bimagnetic nanocrystals in a core–shell architecture has been synthesized, and their magnetic properties have been systematically studied. Both HRTEM and EDS results confirmed the formation of bimagnetic core–shell structured nanocrystals. On the basis of the systematic and comparative studies of the magnetic properties of a mechanical mixture of pure $CoFe_2O_4$ and $MnFe_2O_4$ nanocrystals, chemically mixed $Co_{1-x}Mn_xFe_2O_4$ nanocrystals, and bimagnetic core–shell $CoFe_2O_4$@$MnFe_2O_4$ and $MnFe_2O_4$@$CoFe_2O_4$ nanocrystals, the bimagnetic core–shell nanocrystals show very unique magnetic properties, such as the blocking temperature and coercivity. Our results show that the coercivity correlates with the volume fraction of the soft phase as the theoretical hard–soft phase model has suggested. Furthermore, switching the hard phase $CoFe_2O_4$ from the core to the shell shows great changes in the coercivity of the nanocrystals. The bimagnetic core–shell nanocrystals evidently demonstrate the rational design capability to separately control the blocking temperature and the coercivity in magnetic nanocrystals by varying the materials, their combination, and the volume ratio between the core and the shell and by switching hard or soft phase materials between the core and shell. Such controls via a bimagnetic core–shell architecture are highly desirable for magnetic nanocrystals in various applications.

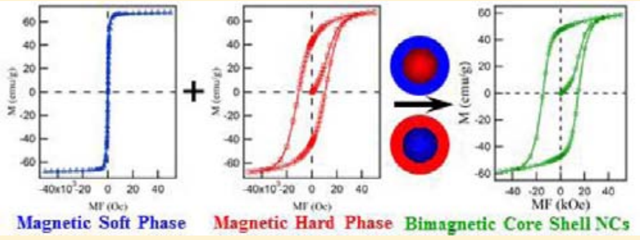

■ INTRODUCTION

Core–shell architecture has been extensively studied in a wide variety of nanomaterials. In addition to varying size, shape, and composition,[1−4] this approach becomes a prevailing strategy, introducing a new variable for the rational material design and property control in fundamental science and technological applications.[5−46] For magnetic nanomaterials, the core–shell architecture enables us to independently address the competing technical demands on the magnetic properties, such as the thermal stability of magnetization and coercivity. Recent studies have demonstrated some merits of bimagnetic core–shell nanocrystals in improving the energy product of permanent magnets[47] and in enhancing the thermal stability of magnetic nanocrystals to overcome the "superparamagnetic limitation" in recording media.[48] Certainly, the exploration of various core–shell combinations of different magnetic materials will provide a better fundamental understanding of magnetic interactions and achieve the desirable magnetic characteristics for specific applications.

Several reports have been published on the magnetic properties of bimagnetic nanocrystals with core–shell architecture produced by the evaporation–deposition, reduction–surface oxidation, and high temperature thermal decomposition methods.[17,23,49,50] For example, the studies of bimagnetic core–shell nanocrystals comprised of a hard phase of FePt core and a soft phase of Fe_3O_4 shell showed that the coercivity is monotonically decreased as the soft phase Fe_3O_4 volume fraction is increased.[17,51,52] A similar reduction of coercivity with increasing amount of soft magnetic material was also reported in other bimagnetic core–shell typed nanoparticles such as $CoFe_2O_4$@$ZnFe_2O_4$, $CoFe_2O_4$@$MnFe_2O_4$, FePt@$CoFe_2O_4$, and $CoFe_2O_4$@$CoFe_2$.[17,23,32,53,54] However, a recent report showed a large increase of coercivity in a bimagnetic Fe_3O_4 core and Mn–Zn ferrite shell cube-shaped nanoparticles[45] and in Fe_xO@$CoFe_2O_4$ bimagnetic core–shell nanoparticles.[55] When the core–shell nanoparticles were formed by coordination compounds of Prussian Blue analogues, $Cs^I[Ni^{II}Cr^{III}(CN)_6]$@$Cs^I[Co^{II}Cr^{III}(CN)_6]$, the coercivity was higher than that of the nanoparticles of either pure $Cs^I[Ni^{II}Cr^{III}(CN)_6]$ or $Cs^I[Co^{II}Cr^{III}(CN)_6]$.[56] Surely, it is almost impossible to draw any definite conclusions regarding the unique magnetic properties in core–shell nanocrystals by comparing these very diverse materials with contradicting properties. A systematic study is essential to understand the magnetic properties of bimagnetic core–shell nanomaterials with a controlled variation of hard and soft magnetic phases.

As one of the most important and widely utilized magnetic materials, the spinel ferrite system consists of both magnetically hard and soft materials. For example, cobalt ferrite ($CoFe_2O_4$) is magnetically hard with a large magnetocrystalline anisotropy constant $k > 10^5 J/m^3$. On the other hand, manganese ferrite ($MnFe_2O_4$) is a typical soft ferrite with a much smaller magnetic anisotropy constant $k \sim 10^3$ J/m^3.[57,58] Due to the

Received: March 23, 2012
Published: May 23, 2012

dx.doi.org/10.1021/ja302856z | *J. Am. Chem. Soc.* 2012, 134, 10182−10190

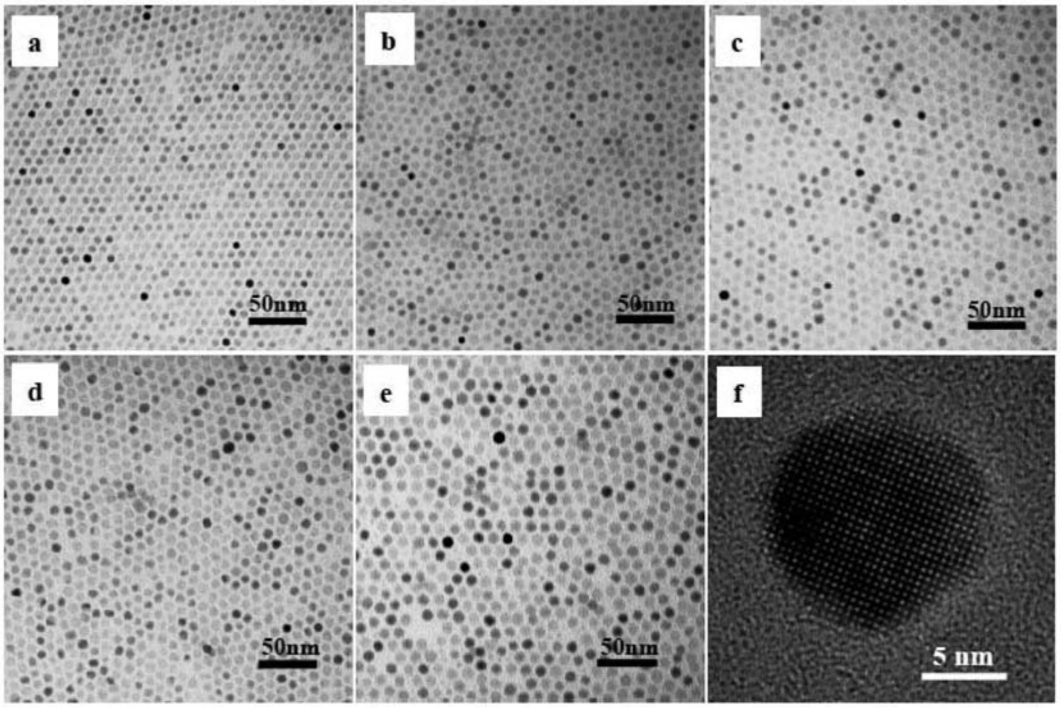

Figure 1. TEM images of 6 nm core $MnFe_2O_4$ nanocrystals (a) and core−shell $MnFe_2O_4$@$CoFe_2O_4$ nanocrystals with shell thicknesses 0.75 nm (b), 1 nm (c), 2 nm (d), and 2.5 nm (e); and HRTEM image (f).

same crystallographic structure and almost negligible lattice mismatch among many different spinel ferrites,[59] it should be markedly controllable to epitaxially grow a uniformed shell over a core. The well-defined single crystalline bimagnetic spinel ferrite nanocrystals with core−shell architecture can provide a better platform for the fundamental understanding of magnetism in the nanoscale regime. Furthermore, there already is a well-established knowledge base on spinel ferrite nanocrystals. Some spinel ferrites nanocrystals such as $CoFe_2O_4$ and $MnFe_2O_4$ have been synthesized and systematically studied regarding their magnetic properties varying with size, shape, surface ligand, interparticle interaction, and electron spin−orbital coupling effects.[60−66]

In this report, we utilized a combination of hard phase $CoFe_2O_4$ and soft phase $MnFe_2O_4$ to clearly demonstrate that the bimagnetic nanocrystals in a core−shell architecture possess unique magnetic characteristics. To prove the distinct magnetic properties of the core−shell structure, we conducted comparative studies on two additional nanoparticulate systems. One is the physical mixture of $CoFe_2O_4$ and $MnFe_2O_4$ nanocrystals, and the other is the chemically mixing of $CoFe_2O_4$ and $MnFe_2O_4$ phases to form a solid solution of $Co_{1-x}Mn_xFe_2O_4$ nanocrystals. The magnetic properties of $CoFe_2O_4$ and $MnFe_2O_4$ core−shell nanocrystals are distinctively different from those of their counterparts in physically and chemically mixing nanoparticulate systems, even though all these nanocrystals were synthesized by the same method. For further understanding the magnetic properties of bimagnetic core−shell nanocrystals, we studied the effect of the volume ratio of magnetic hard and soft phases. We also studied the effect on the magnetic properties of the core−shell nanocrystals by switching roles as core or shell between these two magnetic materials, which were denoted as $CoFe_2O_4$@$MnFe_2O_4$ and $MnFe_2O_4$@$CoFe_2O_4$. Our results clearly show that the magnetic properties, in particular the blocking temperature (T_B) and coercivity (H_C), can be precisely tailored by varying the core and shell materials as well as by controlling the volume fraction of the magnetically soft phase.

■ EXPERIMENTAL SECTION

Synthesis of Bimagnetic $CoFe_2O_4$@$MnFe_2O_4$ and $MnFe_2O_4$@$CoFe_2O_4$ Core−Shell Nanocrystals. The core $CoFe_2O_4$ and $MnFe_2O_4$ nanocrystals were synthesized by the previously reported nonhydrolysis/seed-mediated growth method.[62,66] To prepare a 6 nm $CoFe_2O_4$ core with 1 nm $MnFe_2O_4$ shell bimagnetic nanocrystals, 60 mg of 6 nm $CoFe_2O_4$ nanocrystals was mixed with 0.5 mmol of iron(III) benzoylacetonate, $Fe(bzac)_3$, and 0.25 mmol of manganese(II) benzoylacetonate, $Mn(bzac)_2$ or $Mn(acac)_2$, 5 mmol of 1-octadecanol, 2 mmol of oleic acid, 2 mmol of oleylamine, and 30 mL of phenyl ether or benzyl ether. The solution was then slowly heated up to reflux for 30 min under N_2 gas flow. After the solution was cooled down to room temperature and 30 mL of ethanol was added, the black precipitates were collected by centrifugation. For further purification, the bimagnetic core−shell $CoFe_2O_4$@$MnFe_2O_4$ nanocrystals were washed with a hexane/acetone mix solvent three times. A similar synthetic procedure was used to make inverted $MnFe_2O_4$@$CoFe_2O_4$ core−shell nanocrystals.

Preparation of Physically Mixed $CoFe_2O_4$ and $MnFe_2O_4$ Nanocrystals. The mechanically mixed $CoFe_2O_4$ and $MnFe_2O_4$ samples were prepared by dispersing a proper amount of $CoFe_2O_4$ and $MnFe_2O_4$ nanocrystals in hexane followed by removing hexane under vacuum. All particle size was 6 nm with a size distribution less than 7%. The molar ratios of $CoFe_2O_4$ to $MnFe_2O_4$ are 4.42:1, 1:1, and 1:3.27, respectively.

Synthesis of $Co_{1-x}Mn_xFe_2O_4$ Nanocrystals. A previously reported nonhydrolysis/seed-mediated growth method[62,66] was used to produce chemically mixed $Co_{1-x}Mn_xFe_2O_4$ nanoparticles with the same sizes but different molar concentrations (x) ranging from 0.02 to 0.7. Both cobalt and manganese salts were added together in the synthesis reaction, and the molar ratio of the reactant controls the chemical composition in produced nanocrystals. All particle size was 6.5 nm with a size distribution about 10%.

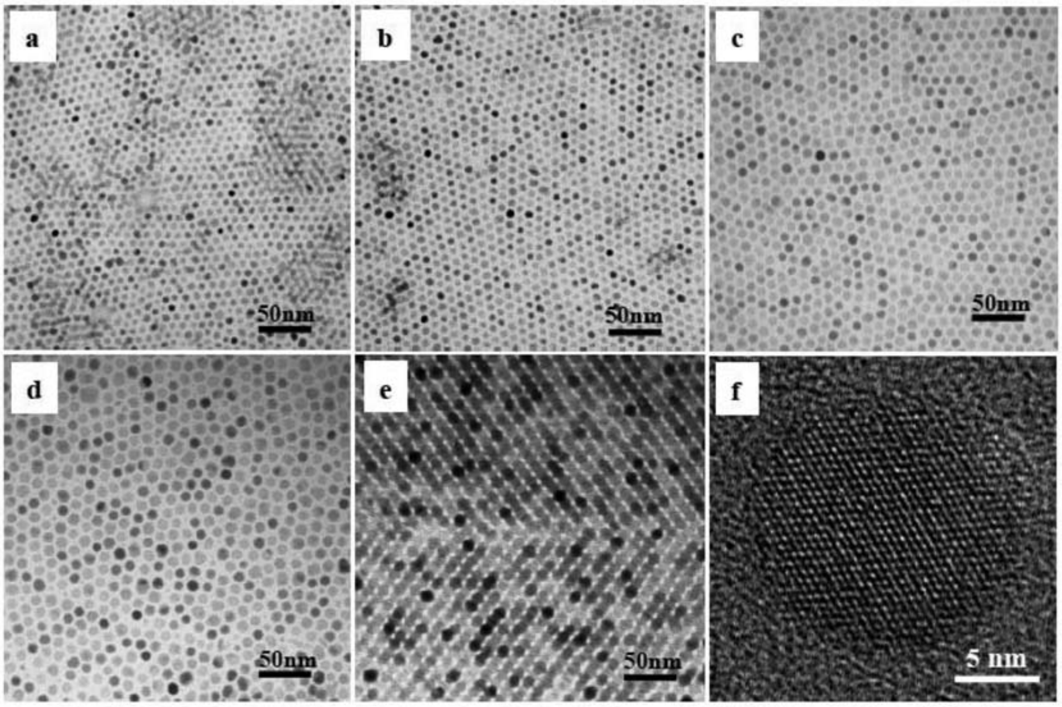

Figure 2. TEM images of 6 nm core $CoFe_2O_4$ nanocrystals (a) and core−shell $CoFe_2O_4$@$MnFe_2O_4$ nanocrystals with shell thickness 0.5 nm (b), 1 nm (c), 2 nm (d), and 3 nm (e); and HRTEM image (f).

Characterizations. Chemical analysis was performed using an inductively coupled plasma atomic emission spectroscopy (ICP-AES) method. Typical transmission electron microscopy (TEM) studies were performed using JEOL 100C operating at 100 kV. Direct measurements of the number of core−shell nanocrystals in TEM micrographs showed a size distribution less than 7%. High-resolution TEM (HRTEM) studies and associated energy dispersive X-ray spectroscopy (EDS) microanalysis were carried out on a Hitachi HF-2000 field emission microscope at 200 kV. A superconducting quantum interference device (SQUID) magnetometer (Quantum Design MPMS-5S) with an applied field up to 5 T was used to measure both temperature and magnetic field dependent magnetizations. The temperature range was varied from 5 to 400 K. All samples for magnetic measurements were prepared by well dispersing a certain amount of dry nanocrystals powder in eicosane (Aldrich, 99%) to eliminate the magnetic interparticle interaction effect.

■ RESULTS AND DISCUSSION

Monodispersed bimagnetic nanocrystals of a $CoFe_2O_4$ core with a $MnFe_2O_4$ shell ($CoFe_2O_4$@$MnFe_2O_4$) and a $MnFe_2O_4$ core with a $CoFe_2O_4$ shell ($MnFe_2O_4$@$CoFe_2O_4$) were synthesized by a combination of a nonhydrolysis reaction and a seed-mediated growth. The shell thickness was systematically tuned from 0.5 to 3 nm. Figure 1 shows the TEM images of $CoFe_2O_4$@$MnFe_2O_4$ nanocrystals with a core diameter of 6 nm and various shell thicknesses.

The TEM images of $MnFe_2O_4$@$CoFe_2O_4$ nanocrystals are displayed in Figure 2 with a 6 nm core and various shell thicknesses. The continuous atomic lattice fringes in high-resolution TEM (HRTEM) images indicate that the shell $CoFe_2O_4$ or $MnFe_2O_4$ is epitaxially overcoated on the respective cores due to a negligible lattice mismatch, and the nanocrystals are highly crystalline single crystals (Figures 1f and 2f). The lack of image contrast between the core and the shell arises from the small difference in electron density between Mn and Co. To verify the formation of core−shell architecture, energy dispersive X-ray spectroscopy (EDS) was used to analyze the chemical composition at the core and the shell sections of $MnFe_2O_4$@$CoFe_2O_4$ and $CoFe_2O_4$@$MnFe_2O_4$ nanocrystals with both a 6 nm core and 1 nm shell, as shown in parts a,b and c,d, respectively, of Figure 3.[67] When the electron beam passed through the center of an individual nanocrystal, all elements of Mn, Fe, Co, and O from both the core and the shell showed up in Figure 3a. In contrast, when the electron beam was carefully aligned through any spot within the shell part, only elements of Co, Fe, and O from the shell were detected, as the representative data show in Figure 3b. The absence of an elemental Mn signal indicates that the shell is formed exclusively by $CoFe_2O_4$. Similarly, the EDS analysis results in Figure 3c,d also clearly confirm the formation of bimagnetic $CoFe_2O_4$@$MnFe_2O_4$ core−shell nanocrystals.

To further confirm that the overall nanocrystals truly have a core−shell architecture, we carried out systematic studies on their magnetic properties to compare with two possible situations. One is that if many $CoFe_2O_4$ or $MnFe_2O_4$ core nanocrystals may not form a core−shell structure, it would lead to a physical mixture of $CoFe_2O_4$ and $MnFe_2O_4$ nanocrystals. The other is that $CoFe_2O_4$ and $MnFe_2O_4$ would diffuse into each other to form a chemically mixed $Co_{1-x}Mn_xFe_2O_4$ system.

A set of the mechanically mixed samples of pure $CoFe_2O_4$ and $MnFe_2O_4$ nanocrystals were used to study the magnetic properties of the mixture of $CoFe_2O_4$ and $MnFe_2O_4$. The molar ratios of $CoFe_2O_4$ to $MnFe_2O_4$ in the mixture were controlled at 4.42:1, 1:1, and 1:3.27, respectively. Their temperature dependent magnetization under 100 Oe magnetic field and their magnetic field dependent magnetization at 5 K are shown in Figure 4.

Figure 5 shows the TEM images of the chemically mixed $Co_{1-x}Mn_xFe_2O_4$ nanocrystals. Direct measurements of these nanocrystals from these TEM images showed that they have a very similar size of 6.5 nm with a 10% size distribution. The

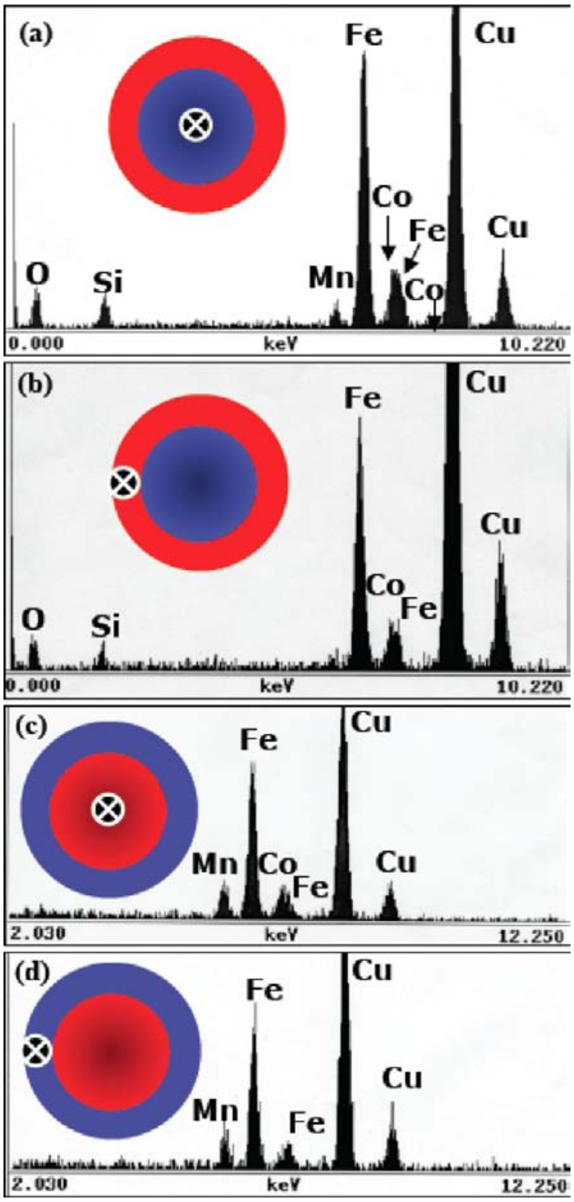

Figure 3. EDS spectra for $MnFe_2O_4@CoFe_2O_4$ (panel a and b) and $CoFe_2O_4@MnFe_2O_4$ (panel c and d) core−shell nanocrystals. The schematic diagrams illustrate where the electron beam was aligned when the corresponding EDS spectrum was acquired.

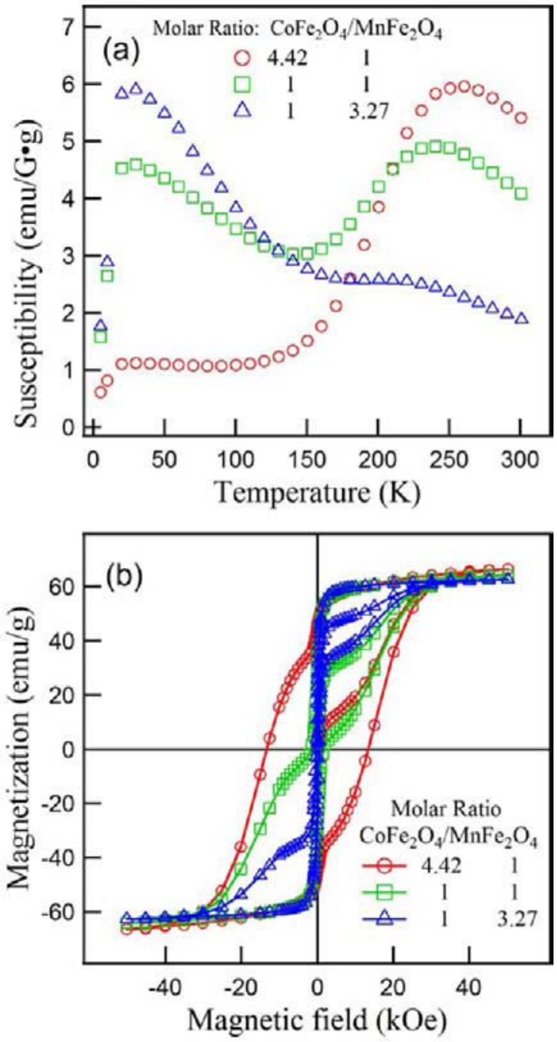

Figure 4. Temperature dependent susceptibility under 100 Oe field (a) and field dependent magnetization at 5 K (b) for physically mixed $CoFe_2O_4$ and $MnFe_2O_4$ nanocrystals.

temperature and magnetic field dependent magnetization for a set of the chemically mixed $Co_{1-x}Mn_xFe_2O_4$ nanocrystals are shown in Figure 6. The chemical composition variation (x) based on Mn molar concentration is controlled from 0.02 to 0.7.

The correlation of the shell thickness with the blocking temperature (T_B) and the coercivity (H_c) of both bimagnetic core−shell $CoFe_2O_4@MnFe_2O_4$ and $MnFe_2O_4@CoFe_2O_4$ nanocrystals was investigated by keeping the same core size (6 nm) while varying the shell thickness from 0.5 to 3 nm. Figure 7a,c shows the temperature dependence of magnetization under a 100 Oe applied magnetic field for both core−shell nanocrystals. The blocking temperature in these two core−shell nanoparticulate systems increases as the shell thickness increases (Figure 7e). The magnetic field dependence of magnetization is displayed in Figure 7b,d. The saturation magnetization and remanent magnetization in both core−shell nanocrystals do not vary much.

However, the coercivity changes significantly as the shell thickness increases. More interestingly, the coercivity increases with the increasing $CoFe_2O_4$ shell thickness in core−shell $MnFe_2O_4@CoFe_2O_4$ nanocrystals. On the contrary, it decreases with increasing $MnFe_2O_4$ shell thickness in $CoFe_2O_4@MnFe_2O_4$ nanocrystals (Figure 7f).

Clearly, the bimagnetic core−shell $CoFe_2O_4@MnFe_2O_4$ and $MnFe_2O_4@CoFe_2O_4$ nanocrystals possess distinct magnetic properties that are far different from those for the physical and chemical mixture of $MnFe_2O_4$ and $CoFe_2O_4$ nanocrystals. The easy comparison is the variations of blocking temperature and coercivity as a function of magnetic $MnFe_2O_4$ component. When pure $MnFe_2O_4$ nanocrystals were mechanically combined with pure $CoFe_2O_4$ nanocrystals to form a physical mixture, the temperature-dependent magnetization shows two distinct peaks at low and high temperature regions (Figure 4a). These two peaks can easily be attributed to the blocking temperatures of $MnFe_2O_4$ and $CoFe_2O_4$ nanocrystals, respectively. The field-dependent magnetization shows a typical two-phase magnetization behavior as a consequence of weak (or none) exchange coupling between hard phase $CoFe_2O_4$ and soft phase $MnFe_2O_4$ nanocrystals (Figure 4b).

The chemically mixed solid solution of $MnFe_2O_4$ and $CoFe_2O_4$ nanocrystals displays uniformed single phase magnetic characteristics. Although this nanoparticulate system itself possesses some unique magnetic properties, these properties are distinctively different from those of the bimagnetic core−shell nanocrystals. The temperature dependent magnetization measurements show a decreasing blocking temperature of $Co_{1-x}Mn_xFe_2O_4$ nanocrystals with increasing molar percent of Mn (Figure 6c). The reason could be that $MnFe_2O_4$ has a much smaller magnetocrystalline anisotropy constant because of very weak electron spin−orbit coupling of the Mn cation. Consequently, as more Mn^{2+} cations substitute for Co^{2+} cations in $CoFe_2O_4$, the blocking temperature decreases. From magnetic field dependent studies, the coercivity is first increased as Mn molar percent is increased from 0.02 to 0.5, and then it is decreased as Mn is further increased to 0.7 (Figure 6d). It is still unclear how to understand such a correlation between the coercivity and the chemical composition in $Co_{1-x}Mn_xFe_2O_4$ nanocrystals. Further systematic studies are needed. Nevertheless, the comparison of the magnetic properties between the core−shell nanocrystals and these physical and chemical mixtures unambiguously supports the TEM-EDS studies on the formation of well-

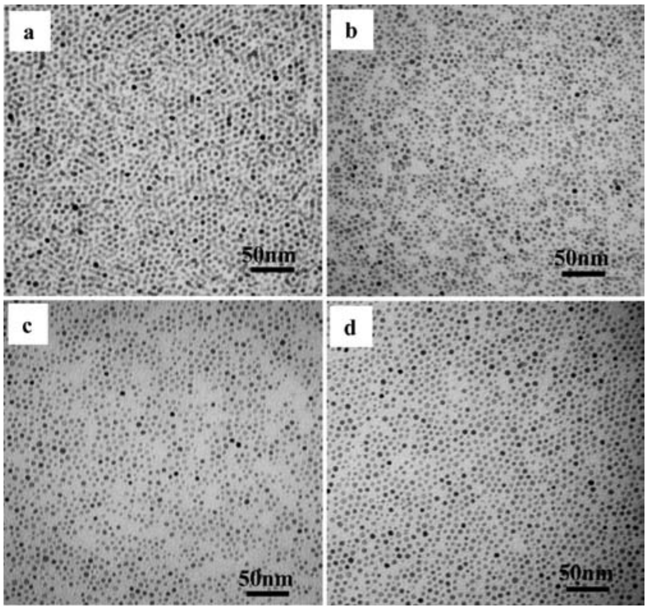

Figure 5. TEM images of $Co_{1-x}Mn_xFe_2O_4$ nanoparticles with X as 0.1 (a), 0.3 (b), 0.5 (c), and 0.7 (d), respectively. The size is about 6.5 nm with a 10% size distribution.

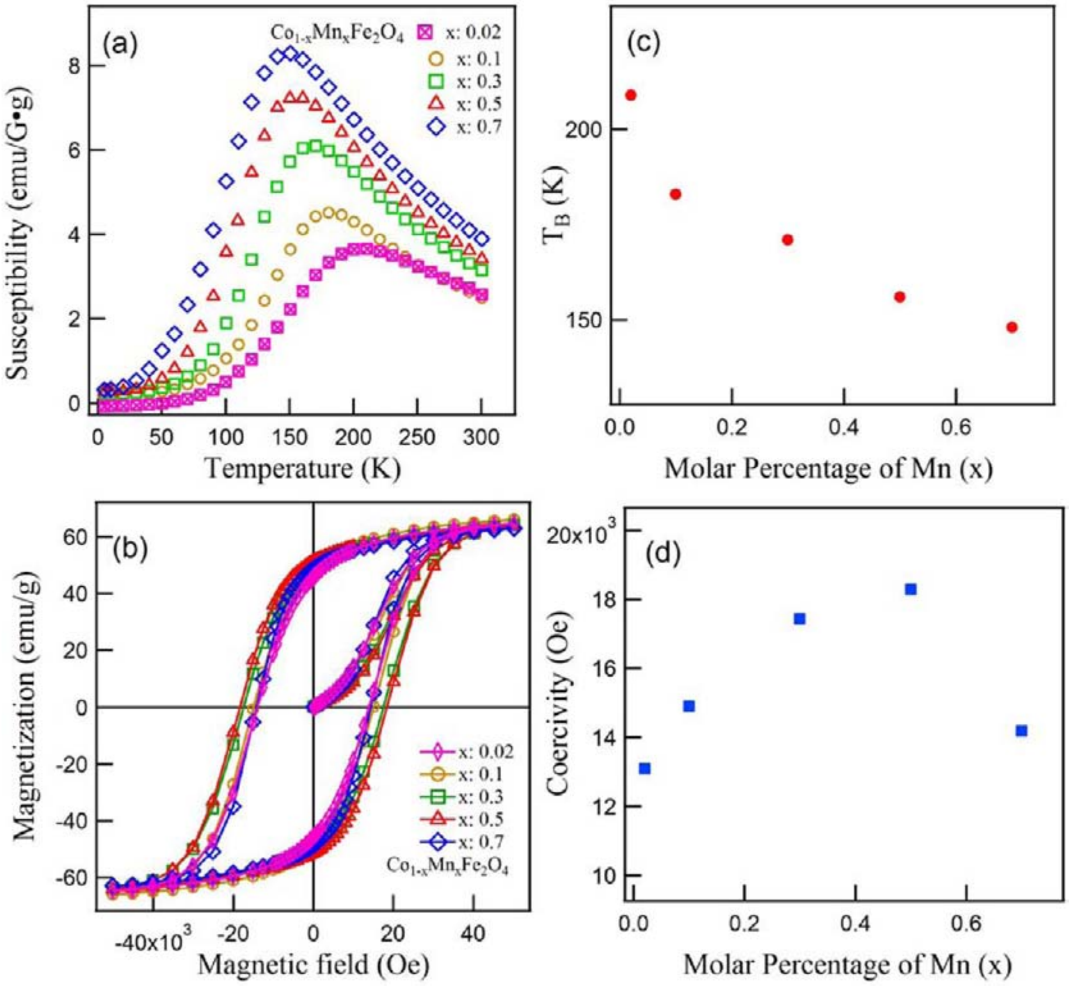

Figure 6. Temperature dependent susceptibility under 100 Oe field (a) and field dependent magnetization at 5 K (b) for 6.5 nm $Co_{1-x}Mn_xFe_2O_4$ nanoparticles. Composition dependences of the blocking temperature and the coercivity are displayed in panels c and d, respectively.

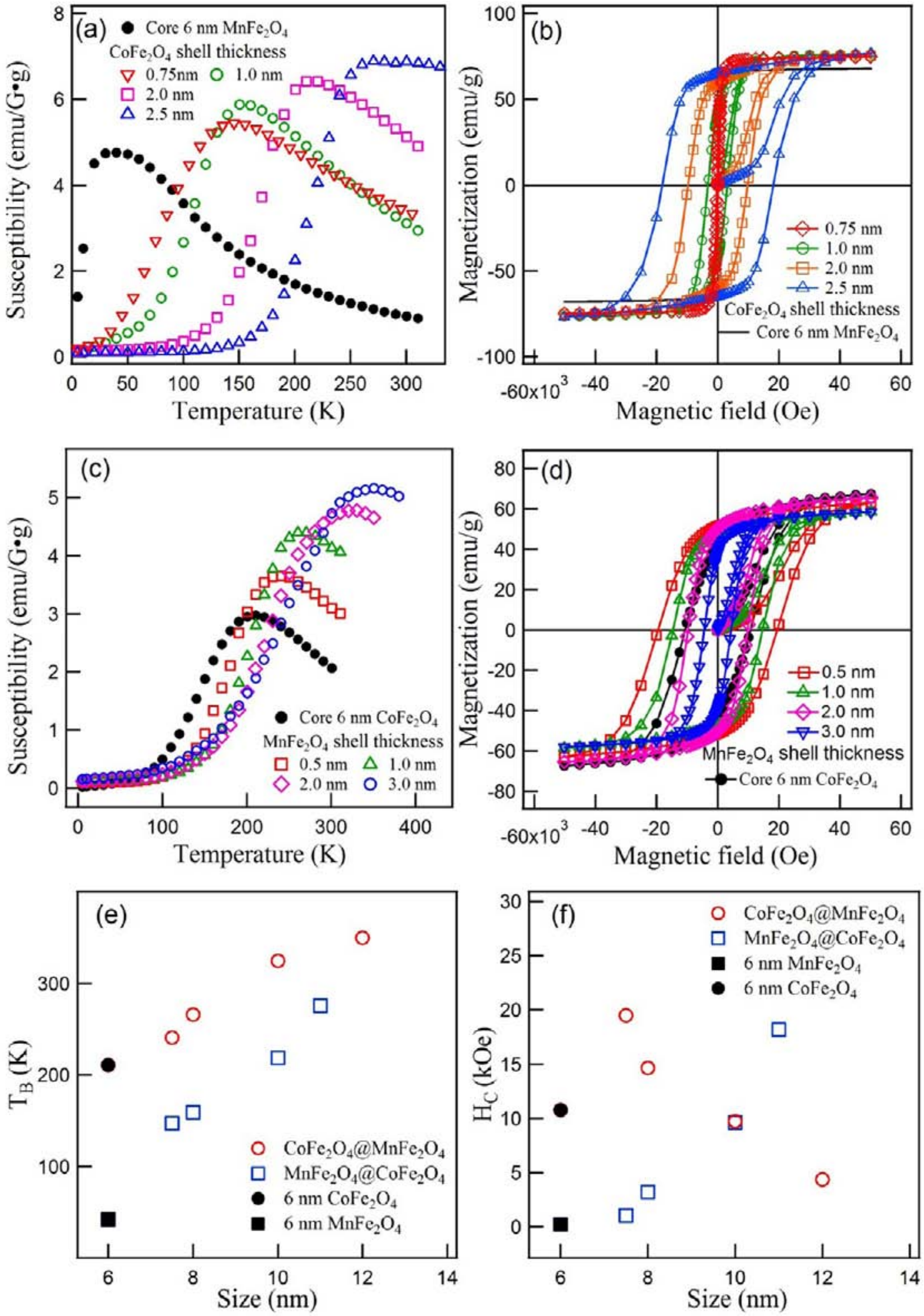

Figure 7. Temperature dependent susceptibility under 100 Oe field and field dependent magnetization at 5 K for $MnFe_2O_4$@$CoFe_2O_4$ (panel a and b) and $CoFe_2O_4$@$MnFe_2O_4$ (panel c and d) core−shell nanocrystals. Shell thickness dependences of the blocking temperature and the coercivity are displayed in panels e and f, respectively.

defined bimagnetic core−shell $CoFe_2O_4$@$MnFe_2O_4$ and $MnFe_2O_4$@$CoFe_2O_4$ nanocrystals.

The unique magnetic properties of bimagnetic core−shell nanocrystals using the same two magnetic materials can be greatly different, when the roles as the core or shell are inverted. As shown in Figure 7e, although the T_B values of both $CoFe_2O_4$@$MnFe_2O_4$ and $MnFe_2O_4$@$CoFe_2O_4$ core−shell nanocrystals increase with increasing shell thickness, the value rises much faster for $MnFe_2O_4$@$CoFe_2O_4$ core−shell nanocrystals than that for $CoFe_2O_4$@$MnFe_2O_4$ ones. Such a discrepancy can be understood by the Stoner−Wohlfarth model,[68] where the magnetic anisotropy energy (E_A) is determined by the magnetocrystalline anisotropy constant (K) and volume (V). Since T_B is correlated to E_A, it thus depends on K and V accordingly. T_B increases in general as the total volume increases with adding more shell volume. The increase of T_B is more drastic by the enhancement of magnetocrystalline anisotropy from the addition of $CoFe_2O_4$ for $MnFe_2O_4$@$CoFe_2O_4$ core−shell nanocrystals, if considering K of $CoFe_2O_4$ is close to 2 orders of magnitude larger than K of $MnFe_2O_4$. The change is very profound even if the shell thickness is only 0.75 nm. Considering the lattice constant is 0.838 nm for a $CoFe_2O_4$ cubic unit cell, the shell thickness of 0.75 nm implies less than even one complete unit cell on the $MnFe_2O_4$ core. It is very possible that the shell is still in the process of formation and does not completely cover the $MnFe_2O_4$ core. The uncertainty associated with a mixed $MnFe_2O_4$ and $CoFe_2O_4$ surface may be the reason for the less than normal temperature dependent magnetization as the core−shell nanocrystals with 0.75 nm shell show in Figure 7a.

The magnetic coercivity studies have shown a significant difference between the core−shell and $Co_{1-x}Mn_xFe_2O_4$ nanocrystals as well as between two different shells in the core−shell nanocrystals. In $Co_{1-x}Mn_xFe_2O_4$ nanocrystals, the coercivity displays an initial increase and then a decrease as the molar ratio of Mn increases. The coercivity decreases in core−shell nanocrystals as the overall molar ratio of Mn increases regardless of whether $MnFe_2O_4$ is the core or the shell. The only increase with $MnFe_2O_4$ observed is the initial addition of a $MnFe_2O_4$ shell on a $CoFe_2O_4$ core. When $MnFe_2O_4$ acts as a shell on the magnetically hard phase $CoFe_2O_4$ core, the coercivity steadily decreases with increasing shell thickness from 10,791 Oe of the core alone to 4,363 Oe for the nanocrystals with 3 nm shell thickness (Figure 7f). After the shell of $CoFe_2O_4$ is formed on a 6 nm $MnFe_2O_4$ core, the coercivity rapidly increases from a magnetically soft state of 221 Oe to a magnetically hard state of 18,175 Oe at the shell thickness of 2.5 nm. Such a straight increase occurs as the molar ratio of Mn relatively decreases, which is consistent with the trend in $CoFe_2O_4$@$MnFe_2O_4$ nanocrystals.

Although bimagnetic core−shell nanocrystals are composed of magnetically hard and soft phases, the magnetic interactions within the bimagnetic core−shell nanocrystals are thoroughly integrated. The temperature-dependent magnetization varies as smoothly as the variation of magnetization in single phase magnetic nanocrystals (Figure 7a,c and Figure 6a). So does the field-dependent magnetization behavior as a single phase hysteresis (Figures 7b,d and 6b). The smooth variations of magnetization imply that the exchange interaction or coupling effectively propagates through the entire bimagnetic core−shell nanocrystal without hindrance. On the basis of some theoretical studies and recent experimental results,[47,51,52,69,70] for an exchange coupled hard−soft magnetic system to coherently respond to the temperature and magnetic field, the hard and soft phases should be intimately orientated, and the thickness of the soft phase should be within twice the domain wall width of the hard phase (δ_W).[58] The domain wall width can be calculated as

$$\delta_W = (A/K_u)^{1/2} \tag{1}$$

where A is the stiffness constant and the magnitude is about ∼1 × 10^{-6} erg/cm; K_u is the uniaxial magnetocrystalline anisotropy constant. For $CoFe_2O_4$, K_u is about 2.6 × 10^6 erg/cm^3. Therefore, Our estimated δ_W of hard phase $CoFe_2O_4$ is about 8 nm. For all bimagnetic core−shell nanocrystals in this work, the shell thickness is much smaller than the 2δ_W of hard phase $CoFe_2O_4$ (16 nm). Therefore, the magnetization of bimagnetic core−shell nanocrystals characteristically resembles that of single phase magnetic nanocrystals.

The coercivity is a measure of reverse field strength to overcome E_A and the surface magnetic anisotropy due to the surface spin pinning.[58,59,71] The trend that the coercivity of bimagnetic core−shell $CoFe_2O_4$@$MnFe_2O_4$ nanocrystals declines with the increasing of the magnetically soft shell is consistent with those previously reported results.[54] According to theoretical study on the exchange-coupled hard−soft two phase composite,[69] the coercivity can be expressed as

$$H_C = 2\frac{K_H f_H + K_S f_S}{M_H f_H + M_S f_S} \tag{2}$$

where K is the anisotropy constant, M is the saturation magnetization, and f is the volume fraction. H and S denote hard and soft phase, respectively. Equation 2 can be further simplified, given the fact that K of $CoFe_2O_4$ is nearly 2 orders of magnitude larger than that of $MnFe_2O_4$, and the difference of M between $CoFe_2O_4$ and $MnFe_2O_4$ is insignificant. Since the coercivity of pure $CoFe_2O_4$ nanocrystals, H_H, can be approximated as $2K_H/M_H$, the new expression for bimagnetic core−shell nanocrystals can be

$$H_C = H_H(1 - f_S) \tag{3}$$

Thus, it is linearly propositional to the volume fraction of the soft phase. For both $CoFe_2O_4$@$MnFe_2O_4$ and $MnFe_2O_4$@$CoFe_2O_4$ core−shell nanocrystals, the coercivity as a function of the volume fraction of soft phase $MnFe_2O_4$ is plotted in Figure 8. In both cases of bimagnetic core−shell nanocrystals, the variation of coercivity has a linear trend with the volume fraction of magnetically soft phase $MnFe_2O_4$. Such results suggest somewhat agreement with the theoretical hard−soft composite model. Certainly, we have to bear in mind that the linear expression in eq 3 is the consequence of an approximation resulting from oversimplifying several parameters.

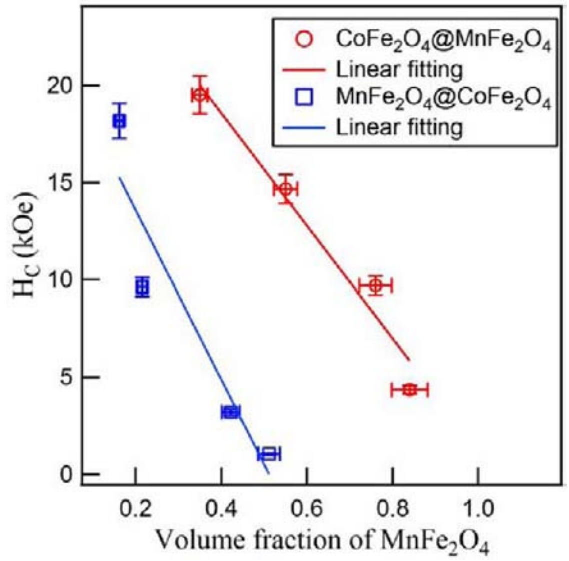

Figure 8. Coercivity of bimagnetic core−shell nanocrystals $CoFe_2O_4$@$MnFe_2O_4$ and $MnFe_2O_4$@$CoFe_2O_4$ as a function of the volume fraction of the magnetically soft phase $MnFe_2O_4$. The solid lines are the linear fittings (○, $CoFe_2O_4$@$MnFe_2O_4$; □, $MnFe_2O_4$@$CoFe_2O_4$).

These results suggest that the model using the volume ratio of hard and soft magnetic phases is very useful but has a severe limitation. The coercivity is dominated by the $CoFe_2O_4$ phase because of its large magnetic anisotropy. However, as Figure 8 shows, it can be dramatically different at the same hard and soft volume ratio if the hard phase switches the role from forming the core to forming the shell. Using the core−shell nanocrystals with an overall diameter of 10 nm as an example, both $CoFe_2O_4$@$MnFe_2O_4$ and $MnFe_2O_4$@$CoFe_2O_4$ nanocrystals have almost the same coercivity of ~9.7 kOe. However, to achieve this coercivity, $CoFe_2O_4$ as the shell requires about 3.6 times the volume in the $MnFe_2O_4$@$CoFe_2O_4$ nanocrystals, as it acts as the core in $CoFe_2O_4$@$MnFe_2O_4$ nanocrystals. This dramatic difference may suggest a different magnetization switching mechanism in the hysteresis loop. When the hard phase $CoFe_2O_4$ forms the shell, it is very possible that its magnetic moments switch directions with those of the curling mechanism through a process of noncoherent rotation to keep them mostly parallel to the particle surface.[72] This mechanism should require much less energy, since it does not need to overcome large electrostatic energy. For the $CoFe_2O_4$ phase in the core, the magnetization switching may go through the Stoner−Wohlfarth coherent rotation mechanism that usually gives a relatively large coercivity. Surely, such speculations can be verified after detailed theoretical and experimental studies. In addition, it is very interesting that the coercivity increased initially when the $MnFe_2O_4$ shell was added onto $CoFe_2O_4$ core nanocrystals even though $MnFe_2O_4$ is magnetically soft. The possible mechanism for this initial increase is unclear, and further studies are needed. The results from this well-defined magnetic spinel system provide an excellent starting point for further theoretical studies on nanomagnetism. From a practical application point of view, it is probably more important to recognize that, besides the size and shape, the coercivity of magnetic nanocrystals can be precisely modulated by the selection of proper hard and soft magnetic materials with a suitable volume ratio via a core−shell architecture. In particular, both the thermal stability associated with the blocking temperature and the magnetic stability related to the coercivity can be decoupled and independently controlled to satisfy the specific application requirements.

■ CONCLUSION

We have demonstrated the controlled synthesis of bimagnetic $CoFe_2O_4$@$MnFe_2O_4$ and $MnFe_2O_4$@$CoFe_2O_4$ core−shell nanocrystals. The bimagnetic core−shell nanocrystals have shown very unique features in both blocking temperature and coercivity. For instance, a T_B of 276 K in $MnFe_2O_4$@$CoFe_2O_4$ nanocrystals with an overall diameter of 11 nm is distinctly different from the T_B of ~110 K and ~320 K for 11 nm pure $MnFe_2O_4$[66] and $CoFe_2O_4$ nanocrystals,[62] respectively. The coercivity even displays more drastic differences. Although the T_B of 11 nm pure $CoFe_2O_4$ nanocrystals is higher than that of the same sized $MnFe_2O_4$@$CoFe_2O_4$ nanocrystals, its coercivity of ~17,000 Oe is smaller. Pure 11 nm $MnFe_2O_4$ nanocrystals only have an H_c of ~370 Oe. The bimagnetic core−shell nanocrystals here evidently demonstrate the rational design capability to separately control the blocking temperature and the coercivity in magnetic nanocrystals by varying the materials, their combination, and the volume ratio between the core and the shell and by switching hard or soft phase materials between the core and shell. Such controls via a bimagnetic core−shell architecture are highly desirable for magnetic nanocrystals in various applications such as high-density storage media, magnetic imaging, sensing, drug delivery, and magnetic hyperthermia.

■ AUTHOR INFORMATION

Corresponding Author

john.zhang@chemistry.gatech.edu

Present Address

[§]IBM Almaden Research Center, 650 Harry Road, San Jose, CA 95120.

Notes

The authors declare no competing financial interest.

■ ACKNOWLEDGMENTS

The authors are grateful to Professor Z. L. Wang for his valuable discussion on EDS measurement and analysis. TEM studies were performed at Georgia Tech Electron Microscopy Center. This research was supported in part by Sandia National Laboratory and the PECASE Program.

■ REFERENCES

(1) Burda, C.; Chen, X.; Narayanan, R.; El-Sayed, M. A. *Chem. Rev.* **2005**, *105*, 1025−1102.
(2) Yin, Y.; Alivisatos, A. P. *Nature* **2005**, *437*, 664−670.
(3) Talapin, D. V.; Lee, J.-S.; Kovalenko, M. V.; Shevchenko, E. V. *Chem. Rev.* **2009**, *110*, 389−458.
(4) Peng, X. *Acc. Chem. Res.* **2010**, *43*, 1387−1395.
(5) Hines, M. A.; Guyot-Sionnest, P. *J. Phys. Chem.* **1996**, *100*, 468−471.
(6) Peng, X.; Schlamp, M. C.; Kadavanich, A. V.; Alivisatos, A. P. *J. Am. Chem. Soc.* **1997**, *119*, 7019−7029.
(7) Cao, Y.-W.; Banin, U. *Angew. Chem., Int. Ed.* **1999**, *38*, 3692−3694.
(8) Cao, Y.; Banin, U. *J. Am. Chem. Soc.* **2000**, *122*, 9692−9702.
(9) Harrison, M. T.; Kershaw, S. V.; Rogach, A. L.; Kornowski, A.; Eychmuller, A.; Weller, H. *Adv. Mater.* **2000**, *12*, 123−125.
(10) Talapin, D. V.; Rogach, A. L.; Kornowski, A.; Haase, M.; Weller, H. *Nano Lett.* **2001**, *1*, 207−211.
(11) Lu, Y.; Yin, Y.; Li, Z.-Y.; Xia, Y. *Nano Lett.* **2002**, *2*, 785−788.
(12) Reiss, P.; Bleuse, J.; Pron, A. *Nano Lett.* **2002**, *2*, 781−784.
(13) Kim, S.; Fisher, B.; Eisler, H.-J.; Bawendi, M. *J. Am. Chem. Soc.* **2003**, *125*, 11466−11467.
(14) Li, J. J.; Wang, Y. A.; Guo, W.; Keay, J. C.; Mishima, T. D.; Johnson, M. B.; Peng, X. *J. Am. Chem. Soc.* **2003**, *125*, 12567−12575.
(15) Talapin, D. V.; Koeppe, R.; Goetzinger, S.; Kornowski, A.; Lupton, J. M.; Rogach, A. L.; Benson, O.; Feldmann, J.; Weller, H. *Nano Lett.* **2003**, *3*, 1677−1681.
(16) Steckel Jonathan, S.; Zimmer John, P.; Coe-Sullivan, S.; Stott Nathan, E.; Bulovic, V.; Bawendi Moungi, G. *Angew. Chem., Int. Ed.* **2004**, *43*, 2154−2158.
(17) Zeng, H.; Li, J.; Wang, Z. L.; Liu, J. P.; Sun, S. *Nano Lett.* **2004**, *4*, 187−190.
(18) Masala, O.; Seshadri, R. *J. Am. Chem. Soc.* **2005**, *127*, 9354−9355.
(19) Xie, R.; Kolb, U.; Li, J.; Basche, T.; Mews, A. *J. Am. Chem. Soc.* **2005**, *127*, 7480−7488.
(20) Zhong, X.; Xie, R.; Zhang, Y.; Basche, T.; Knoll, W. *Chem. Mater.* **2005**, *17*, 4038−4042.
(21) Lee, I. S.; Lee, N.; Park, J.; Kim, B. H.; Yi, Y.-W.; Kim, T.; Kim, T. K.; Lee, I. H.; Paik, S. R.; Hyeon, T. *J. Am. Chem. Soc.* **2006**, *128*, 10658−10659.
(22) Sun, S. *Adv. Mater.* **2006**, *18*, 393−403.
(23) Masala, O.; Hoffman, D.; Sundaram, N.; Page, K.; Proffen, T.; Lawes, G.; Seshadri, R. *Solid State Sci.* **2006**, *8*, 1015−1022.
(24) Yang, Y.; Chen, O.; Angerhofer, A.; Cao, Y. C. *J. Am. Chem. Soc.* **2006**, *128*, 12428−12429.

(25) Ivanov, S. A.; Piryatinski, A.; Nanda, J.; Tretiak, S.; Zavadil, K. R.; Wallace, W. O.; Werder, D.; Klimov, V. I. *J. Am. Chem. Soc.* **2007**, *129*, 11708−11719.

(26) Protiere, M.; Reiss, P. *Small* **2007**, *3*, 399−403.

(27) Xu, Z.; Hou, Y.; Sun, S. *J. Am. Chem. Soc.* **2007**, *129*, 8698−8699.

(28) Blackman, B.; Battaglia, D.; Peng, X. *Chem. Mater.* **2008**, *20*, 4847−4853.

(29) Kim, J.; Rong, C.; Lee, Y.; Liu, J. P.; Sun, S. *Chem. Mater.* **2008**, *20*, 7242−7245.

(30) Peng, S.; Xie, J.; Sun, S. *J. Solid State Chem.* **2008**, *181*, 1560−1564.

(31) Wang, C.; Daimon, H.; Onodera, T.; Koda, T.; Sun, S. *Angew. Chem., Int. Ed.* **2008**, *47*, 3588−3591.

(32) Chaubey, G. S.; Nandwana, V.; Poudyal, N.; Rong, C.-b.; Liu, J. P. *Chem. Mater.* **2008**, *20*, 475−478.

(33) Ge, J.; Zhang, Q.; Zhang, T.; Yin, Y. *Angew. Chem., Int. Ed.* **2008**, *47*, 8924−8928.

(34) Bhattacharyya, S.; Estrin, Y.; Moshe, O.; Rich, D. H.; Solovyov, L. A.; Gedanken, A. *ACS Nano* **2009**, *3*, 1864−1876.

(35) Bodnarchuk, M. I.; Kovalenko, M. V.; Groiss, H.; Resel, R.; Reissner, M.; Hesser, G.; Lechner, R. T.; Steiner, W.; Schaeffler, F.; Heiss, W. *Small* **2009**, *5*, 2247−2252.

(36) Casavola, M.; Falqui, A.; Garcia, M. A.; Garcia-Hernandez, M.; Giannini, C.; Cingolani, R.; Cozzoli, P. D. *Nano Lett.* **2009**, *9*, 366−376.

(37) Deka, S.; Quarta, A.; Lupo, M. G.; Falqui, A.; Boninelli, S.; Giannini, C.; Morello, G.; De Giorgi, M.; Lanzani, G.; Spinella, C.; Cingolani, R.; Pellegrino, T.; Manna, L. *J. Am. Chem. Soc.* **2009**, *131*, 2948−2958.

(38) Li, L.; Daou, T. J.; Texier, I.; Kim Chi, T. T.; Liem, N. Q.; Reiss, P. *Chem. Mater.* **2009**, *21*, 2422−2429.

(39) Narayanaswamy, A.; Feiner, L. F.; Meijerink, A.; van der Zaag, P. J. *ACS Nano* **2009**, *3*, 2539−2546.

(40) Wood, V.; Halpert, J. E.; Panzer, M. J.; Bawendi, M. G.; Bulovic, V. *Nano Lett.* **2009**, *9*, 2367−2371.

(41) Zhang, J.; Tang, Y.; Weng, L.; Ouyang, M. *Nano Lett.* **2009**, *9*, 4061−4065.

(42) Chen, D.; Zhao, F.; Qi, H.; Rutherford, M.; Peng, X. *Chem. Mater.* **2010**, *22*, 1437−1444.

(43) Mazumder, V.; Chi, M.; More, K. L.; Sun, S. *J. Am. Chem. Soc.* **2010**, *132*, 7848−7849.

(44) McKiernan, M.; Zeng, J.; Ferdous, S.; Verhaverbeke, S.; Leschkies, K. S.; Gouk, R.; Lazik, C.; Jin, M.; Briseno, A. L.; Xia, Y. *Small* **2010**, *6*, 1927−1934.

(45) Wang, L.-Y.; Wang, X.; Luo, J.; Wanjala, B. N.; Wang, C.-M.; Chernova, N. A.; Engelhard, M. H.; Liu, Y.; Bae, I.-T.; Zhong, C.-J. *J. Am. Chem. Soc.* **2010**, *132*, 17686−17689.

(46) Zhang, J.; Tang, Y.; Lee, K.; Ouyang, M. *Science* **2010**, *327*, 1634−1638.

(47) Zeng, H.; Li, J.; Liu, J. P.; Wang, Z. L.; Sun, S. *Nature* **2002**, *420*, 395−398.

(48) Skumryev, V.; Stoyanov, S.; Zhang, Y.; Hadjipanayis, G.; Givord, D.; Nogues, J. *Nature* **2003**, *423*, 850−853.

(49) Duxin, N.; Stephan, O.; Petit, C.; Bonville, P.; Colliex, C.; Pileni, M. P. *Chem. Mater.* **1997**, *9*, 2096−2100.

(50) Carpenter, E. E.; Calvin, S.; Stroud, R. M.; Harris, V. G. *Chem. Mater.* **2003**, *15*, 3245−3246.

(51) Zeng, H.; Sun, S.; Li, J.; Wang, Z. L.; Liu, J. P. *Appl. Phys. Lett.* **2004**, *85*, 792−794.

(52) Nandwana, V.; Chaubey, G. S.; Yano, K.; Rong, C. B.; Liu, J. P. *J. Appl. Phys.* **2009**, *105*, 014303.

(53) Soares, J. M.; Cabral, F. A. O.; de Araujo, J. H.; Machado, F. L. A. *Appl. Phys. Lett.* **2011**, *98*, 072502.

(54) Lee, J.-H.; Jang, J.-T.; Choi, J.-S.; Moon, S. H.; Noh, S.-H.; Kim, J.-W.; Kim, J.-G.; Kim, I.-S.; Park, K. I.; Cheon, J. *Nature Nanotechnol.* **2011**, *6*, 418−422.

(55) Pichon, B. P.; Gerber, O.; Lefevre, C.; Florea, I.; Fleutot, S.; Baaziz, W.; Pauly, M.; Ohlmann, M.; Ulhaq, C.; Ersen, O.; Pierron-Bohnes, V.; Panissod, P.; Drillon, M.; Begin-Colin, S. *Chem. Mater.* **2011**, *23*, 2886−2900.

(56) Catala, L.; Brinzei, D.; Prado, Y.; Gloter, A.; Stephan, O.; Rogez, G.; Mallah, T. *Angew. Chem., Int. Ed.* **2009**, *48*, 183−187.

(57) *Handbook of Magnetic Materials*; Buschow, K. H. J., Ed.; Elsevier: 1995; Vol. *8*.

(58) O'Handley, R. C. *Modern Magnetic Materials: Principles and Applications*; John Wiley & Sons: New York, 2000.

(59) Cullity, B. D.; Graham, C. D. *Introduction to Magnetic Materials*, 2nd ed.; John Wiley & Sons: Hoboken, 2009.

(60) Vestal, C. R.; Zhang, Z. J. *J. Am. Chem. Soc.* **2002**, *124*, 14312−14313.

(61) Vestal, C. R.; Zhang, Z. J. *J. Am. Chem. Soc.* **2003**, *125*, 9828−9833.

(62) Song, Q.; Zhang, Z. J. *J. Am. Chem. Soc.* **2004**, *126*, 6164−6168.

(63) Vestal, C. R.; Song, Q.; Zhang, Z. J. *J. Phys. Chem. B* **2004**, *108*, 18222−18227.

(64) Song, Q.; Ding, Y.; Wang, Z. L.; Zhang, Z. J. *J. Phys. Chem. B* **2006**, *110*, 25547−25550.

(65) Song, Q.; Zhang, Z. J. *J. Phys. Chem. B* **2006**, *110*, 11205−11209.

(66) Song, Q.; Ding, Y.; Wang, Z. L.; Zhang, Z. J. *Chem. Mater.* **2007**, *19*, 4633−4638.

(67) Li, J.; Zeng, H.; Sun, S.; Liu, J. P.; Wang, Z. L. *J. Phys. Chem. B* **2004**, *108*, 14005−14008.

(68) Stoner, E. C.; Wohlfarth, E. P. *Trans. R. Soc.* **1948**, *A240*, 599−644.

(69) Skomski, R.; Coey, J. M. D. *Phys. Rev. B: Condens. Matter* **1993**, *48*, 15812−15816.

(70) Skomski, R.; Coey, J. M. D. *IEEE Trans. Magn.* **1994**, *30*, 607−609.

(71) Dormann, J. L.; Fiorani, D.; Tronc, E. *Adv. Chem. Phys.* **1997**, *98*, 283−494.

(72) Brown, W. F., Jr. *Phys. Rev.* **1957**, *105*, 1479−1482.